Electronic Supplementary Material (ESI) for ChemComm.

Supporting Information

Self-assembled Monolayer Functionalized NiO Nanowires: Strategy to Enhance the Sensing Performance of p-type Metal Oxide

Navpreet Kaur[a], Mandeep Singh[a,b]*, Andrea Casotto[c,d], Luigi Sangaletti[c] and Elisabetta Comini[a]*

[a]SENSOR Laboratory, University of Brescia and INSTM Udr Brescia, Via D. Valotti 9, Brescia 25133, Italy

[b]Department of Physics, Politecnico Di Milano, Milano 20133, Itlay

[c]I-LAMP and Dipartimento di Matematica e Fisica, Università Cattolica del Sacro Cuore, via della Garzetta 48, Brescia 25133, Italy

[d]Department of Chemistry and Biochemistry, University of Notre Dame, Notre Dame, IN 46556, USA

Table of Content

1.1. NiO NWs growth using VLS Mechanism

In the present work, 3×3mm^2 alumina substrates (99% purity, Kyocera, Japan) were used to grow the NiO nanowires (NWs). Prior to the NWs growth, substrates were ultrasonically cleaned with acetone for 20 minutes and then dried with synthetic air. Afterward, gold (Au) catalyst was deposited on the alumina substrates using RF-magnetron sputtering. The catalyst deposition was done at 70 watts with 7 sccm of argon (Ar) plasma for 5 seconds. The Au catalysts acted as nucleation sites for the growth of highly crystalline nanowires. Indeed, during the growth, these metal catalysts liquidized and when the supersaturation was reached, acted as a preferential sites for the crystallization of nanowires.[1] It should be pointed out that the middle area of the alumina substrate were exposed to Au-catalyst and the sides were masked for the deposition of Pt-contacts.

Furthermore, NiO NWs growth was performed in a lab-made tubular furnace equipped with vacuum pumps and heating system by using vapor liquid solid (VLS) mechanism (figure S1). The vacuum pump maintains a pressure of 1 mbar inside the alumina tube during the deposition. The NiO powder (Sigma Aldrich) was placed inside the furnace in the maximum temperature region i.e. at 1400 °C to promote evaporation. While the substrates were placed at a temperature of 930 °C since a colder region is necessary to promote the NiO vapors condensation.[2] The deposition was carried out for 15 minutes and argon flow (set at 100 sccm) was used as a carrier gas transporting NiO particles form source materials to substates during the deposition. First of all, the furnace was heated up to reach the deposition temperature of 1400°C. In this stage the argon gas flow was maintained from substrates to surface materials direction to avoid any undesired deposition. When the furnace reached the deposition temperature, the argon flow was directed from source to substrate. Indeed, the VLS mechanism is named after the three different phases of material involved in the growth process: vapor state of the source material (NiO), formation of liquid catalyst droplet (Au), and the solid crystalline nanostructure that is produced.[3] Hence, in the present case, the formation of a liquid droplet of a Au-catalyst occurs at substrate temperature of 930°C and NiO vapors adsorb on its surface. Since vapors are continuously provided, the liquid alloy starts to saturate forming a solid precipitate, which grows in the form of 1D nanostructure.[4]

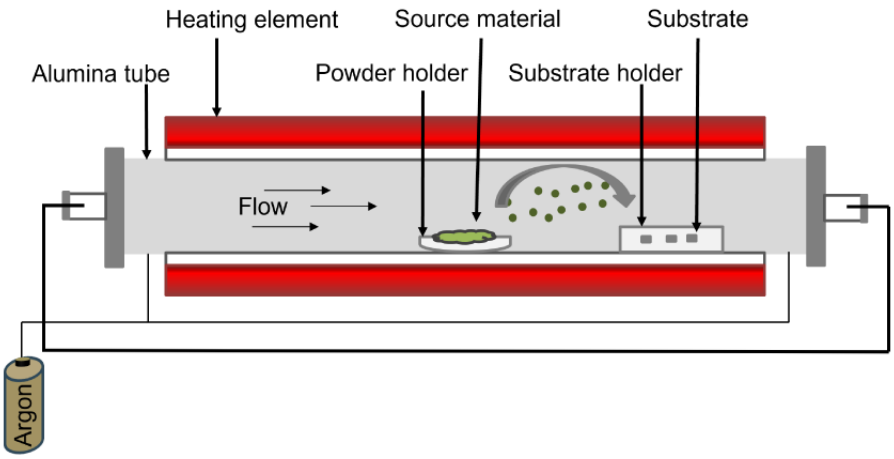

Figure S1. The Schematic diagram of growth setup (Tubular Furnace), b) picture of mounted sensing device.

1.2. Surface functionalization of NiO NWs with self-assembled monolayer

The NiO NWs were functionalized with 3-glycidoxypropyltrimethoxysilane (GOPS) monolayer, which is an organosilanes. Since organosilanes require hydroxyl (—OH) groups on the surface of the interacting material for the monolayer formation,[5] NiO NWs were immersed in 0.2M KOH (potassium hydroxide, Sigma Aldrich) solution in HPLC-grade water (Sigma Aldrich) for 2 hours. Afterward, NWs were taken out from the solution and rinsed extensively with water and ethanol (also dried with synthetic air). Finally, these hydroxylated NiO NWs were dipped inside the 40mM solution of GOPS in anhydrous ethanol for 18 hours at room temperature. During the monolayer formation process, GOPS molecules bind to the hydroxylated-NiO NWS via the formation of polysiloxane bonds that are connected to the surface silanol groups (—SiOH) via Si—O—Si bonds.[1,5] Generally speaking, SAM formation process can be divided into two steps. In the first step, which is extremely quick (a few minutes), a thin monolayer is formed on the surface due to the adsorption of SAM molecules from the bulk solution. While second step involves the rearrangement and reorientation of the adsorbed SAM molecules. This process occurs at a very slow rate (it takes approximately 10–20 hours) in order to achieve highly ordered structures.[5] Hence, after the completion of the SAM formation process (18 hours), the NiO NWs were taken out from the solution and rinsed extensively with ethanol to remove the physically adsorbed GOPS entities. Furthermore, SAM functionalized NWs were annealed at 90 ^{o}C to evaporate the residual solvent. Lastly, epoxy terminated-NiO NWs (NGP) were obtained and used for conductometric device fabrication. The whole process of GOPS SAM formation on NiO NWs surface is depicted in figure S2.

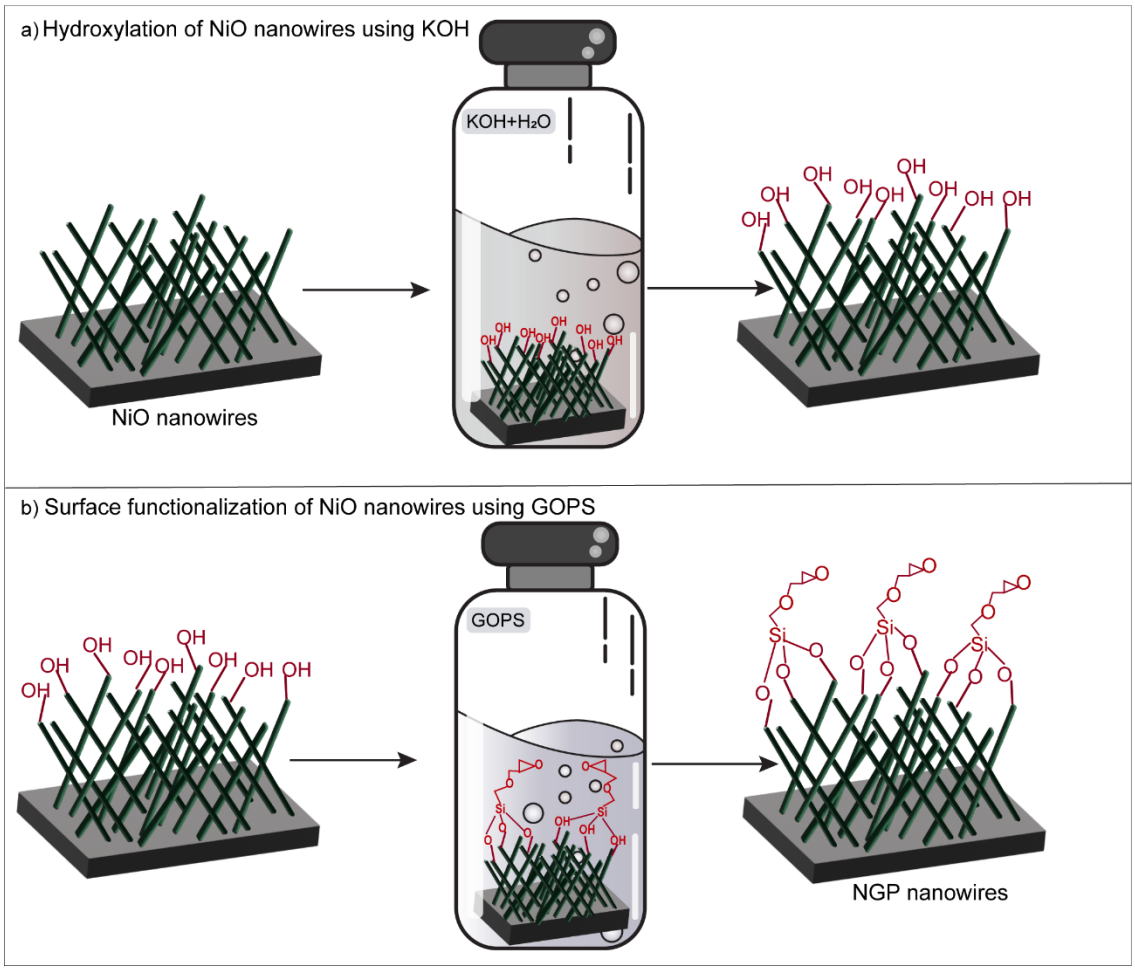

Figure S2. a) Hydroxylation of NiO nanowires in a solution of KOH and water using the dip method. b) functionalization of NiO nanowires after hydroxylation with GOPS.

1.3. Characterization of bare and functionalized NiO nanowires

A field-emission scanning electron microscope MIRA3 LMU (TESCAN, Brno, Czech Republic) was used to investigate the morphology of the NiO NWs. X-ray diffraction (GI-XRD) was performed using an Empyrean diffractometer (PANalytical, Almelo, The Netherlands), mounting a Cu-LFF (λ = 1.5406 Å) tube and operated at 40 kV–40 mA. Spectra were obtained in the Bragg-Brentano geometry, using a linear PIXcel 1D with a large-β nickel filter and recorded in the 30–70° range. Raman spectra were measured by using an XploRA Nano system (Horiba Jobin Yvon Srl, Italy) formed by a confocal microscope (Olympus BX) and an 1800 gr/mm reticule. A Peltier-cooled Open Electrode CCD was used to record the Raman spectra excited by a 638 solid-state laser, in the wavenumber range 200–1800 cm^{-1}. XPS data were collected by using the Al Kα line (hν = 1486.6 eV) from a twin anode X-ray source and a fully calibrated VG-Scienta R3000 spectrometer, with an overall resolution of 0.9 eV.

1.4. Sensor device fabrication

DC magnetron sputtering was used for the fabrication of bare NiO and NGP sensing devices. TOP: Platinum (Pt) interdigitated electrodes (IDEs) and Backside: Pt heating element was deposited by a two-step procedure. The two-step procedure consists of: a) deposition of 50nm thick TiW adhesion layer by DC magnetron sputtering (70 W Ar plasma, 100 nm, ≈ 5.3 × 10^{-3} mbar at RT); b) Pt electrodes, using the same parameters used for the adhesion layer (thickness≈1 µm). Devices were finally mounted on transistor outline (TO) packages using electro-soldered gold wires as shown in figure S3.

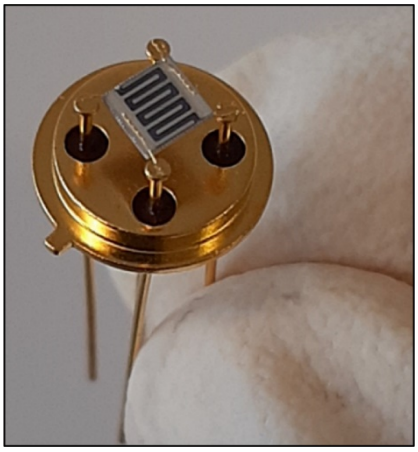

Figure S3. Picture of mounted sensing device.

1.5. Gas Sensing Characterization

Gas sensing tests were performed in a sealed climatic chamber with a constant synthetic airflow [rate = 200 standard cubic centimeters per minute (SCCM) at atmospheric pressure, used as a gas carrier. The atmosphere composition was controlled using mass flow controllers (MKS, Germany), mixing flows coming from certified gas bottles (SOL, Italy) containing a precise concentration of target analytes diluted in synthetic air. The output signal was measured by applying a constant bias of 1 V to the sensing materials, recording the output current using a picoammeter (Keithley, USA). Prior to gas sensing measurements, all sensors were thermally stabilized at the desired working temperature for 6 hours. The response was determined by the variation of conductance using the following formulas, considering a p-type metal oxide for reducing,[2]

$$Response = \frac{G_{air} - G_{gas}}{G_{gas}} \qquad S1$$

And oxidizing gases,

$$Response = \frac{G_{gas} - G_{air}}{G_{air}} \qquad S2$$

where G_{gas} and G_{air} are respectively the sensor conductance in presence of gas, and in synthetic air. Different concentrations of gas analytes such as ethanol, acetone, hydrogen, nitrogen dioxide and methane were tested during the sensing measurements. Further, the experimental data from calibration curves were fitted by typical power trend relations for metal oxides sensors,[6]

$$Response = A(gas\ concetration)^{B} \qquad S3$$

Where, A and B are constants typical of sensor the material and stoichiometry of the involved reaction. The detection limits for the target gases (ethanol and acetone) was calculated by considering by considering a minimum response as 1 to have detectable signal.

1.6. Surface morphology and structural characterization

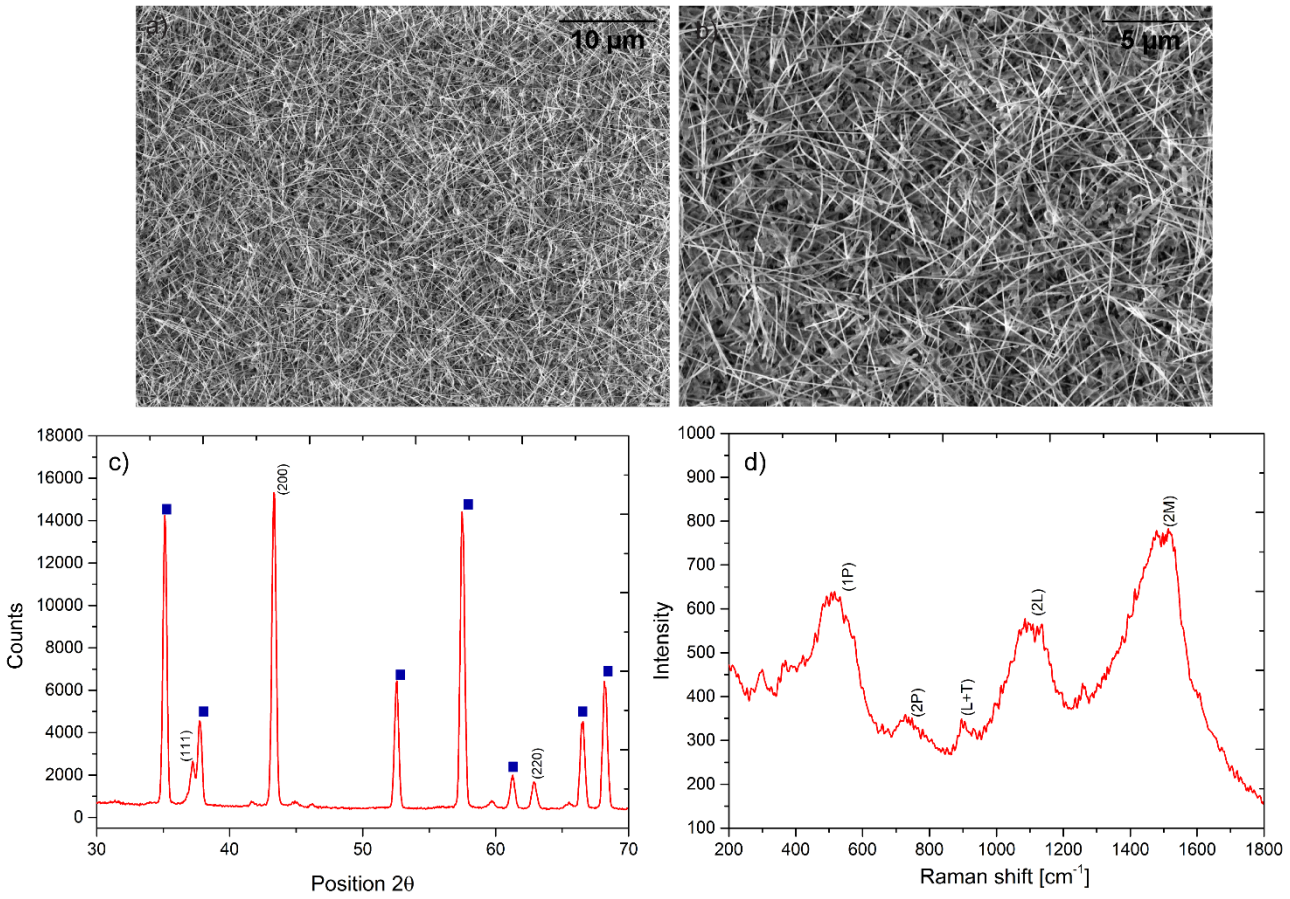

Figure S4. (a, b) SEM images of NiO NWs grown on alumina substrate (diameter was found between 15 nm to 70 nm). c) GI-X-ray diffraction spectra of NiO measured using Cu-LFF source. The diffraction peaks observed at 37.27°, 44.5° and 62.91°, can be indexed to (111), (200) and (220) face centered cubic NiO orientations, respectively. Peaks observed in GI-XRD spectra belong to the bunsenite crystalline structure of NiO nanowires.[2] The extra peaks in the spectra, indicated by blue ticks, are ascribed to the alumina substrate. d) Raman spectra of NiO nanowires sample at room temperature. The peaks shown in the spectrum are assigned to both longitudinal and transverse modes; one phonon (1P) at 570 cm^{-1}, two phonon (2P) transverse modes at ~750 cm^{-1}, longitudinal and transverse modes at ~900 cm^{-1}, and 2Plongitudinal modes at ~1090 cm^{-1}. Furthermore, a peak due to two magnon scattering was observed at ~1490 cm^{-1}.[2,7] All the less intense peaks observed before 450 cm^{-1} belong to the alumina substrate.

1.7. Survey scan XPS spectra of bare and functionalized NiO NWs

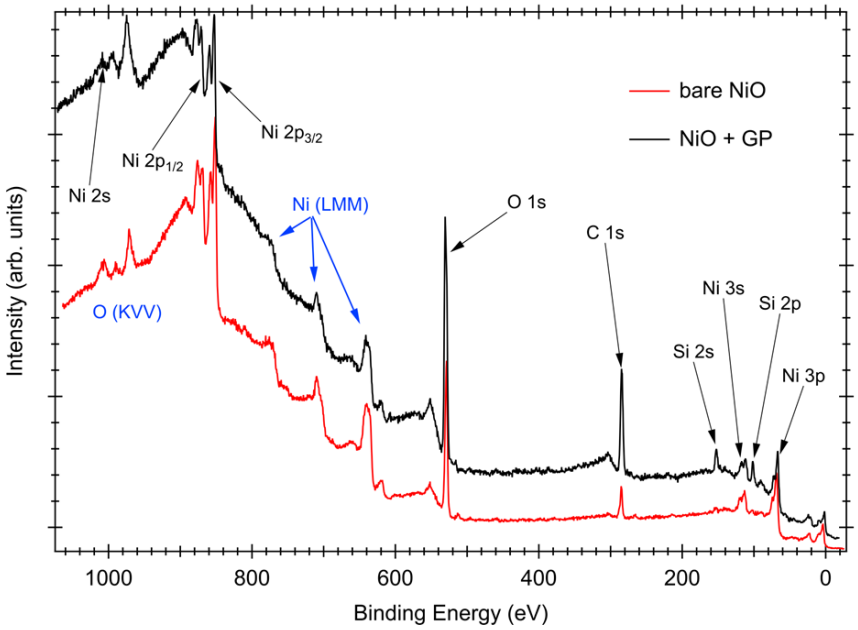

Figure S5. XPS survey spectra of bare and GOPS-functionalized NiO nanowires. The principal core level signals are indicated by arrows, while blue annotations point out the Auger signals' regions. The intensity is normalized on the Ni 3p peak.

Table S1. Elemental quantification obtained from the integration of XPS survey spectra core level signals. Specifically, the elemental quantification was done through the integration of each peak area, followed by the addition of their respective sensitivity factor and the calculated escape depth correction for the NiO[8] (with an error of about 10%).

Elemental Quantification	**Ni**	**O**	**C**	**Si**
NiO	33.9 %	49.5 %	16.6 %	/
NGP	11.5 %	40.6 %	41.7 %	6.2 %

1.8. Dynamic response of bare NiO NWs at 500 °C

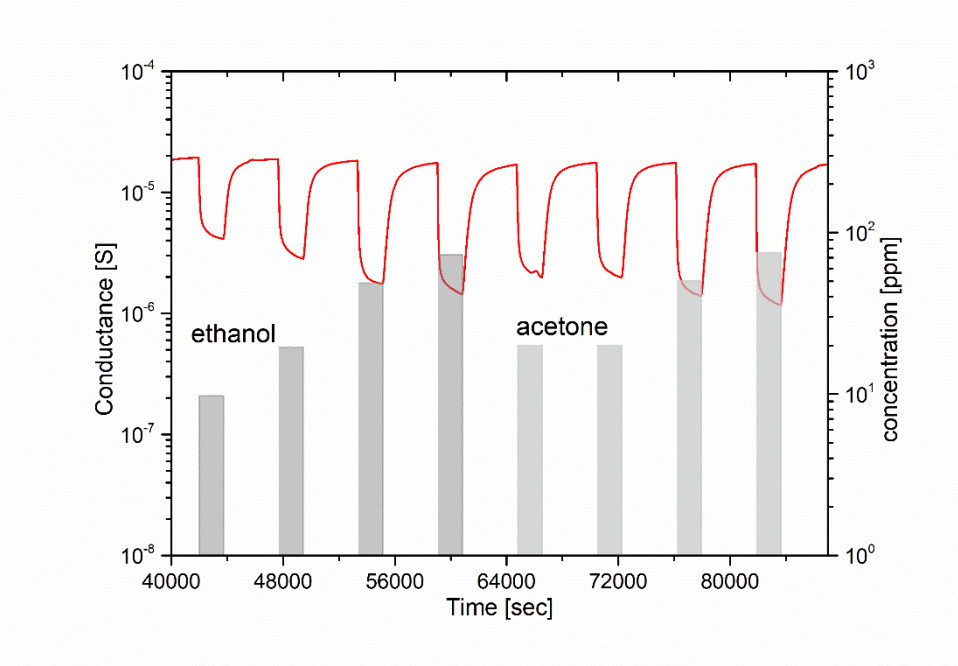

Figure S6: Dynamic response curve of bare NiO nanowires toward different concentrations of acetone and ethanol at 500 °C.

Table S2. Detection limits of NGP and NiO sensors.

Sensor	A	B	Detection limit
NGP_ethanol 200 °C	1.02	0.6	0.9 ppm
NGP_acetone 200 °C	0.3	0.9	3 ppm
NGP_ethanol 150 °C	0.8	0.4	1.8 ppm
NGP_acetone 150 °C	0.2	0.9	9 ppm
NiO_ethanol 200 °C	0.8	0.2	2.3 ppm
NiO_acetone 200 °C	0.2	0.5	16 ppm

1.9. Response and recovery time

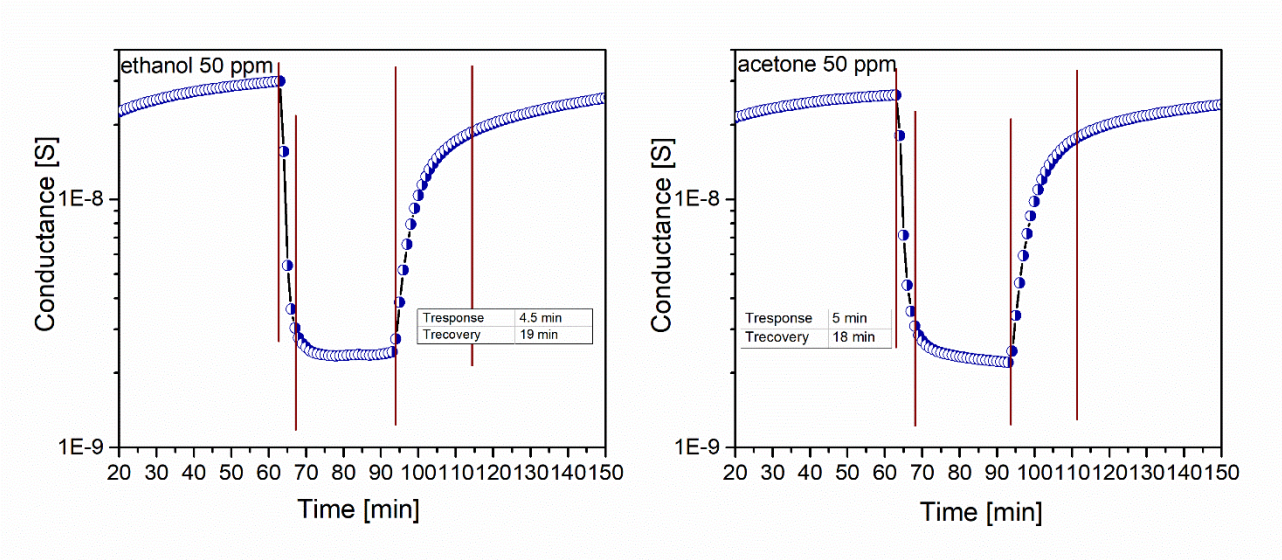

Figure S7: Response and recovery time of NGP sensor towards ethanol and acetone [50 ppm] at 200 °C. The response and recovery time of the sensor was calculated when the response reach 90 % and recovery at 70 %. Indeed, both these values are overestimated because of the limitations of the test chamber which required 5-10 minutes to fill the full volume (1L) of stainless-steel chamber. Thus, in a real much lesser values can be expected for both response and recovery times.

1.10. Humidity and Stability response

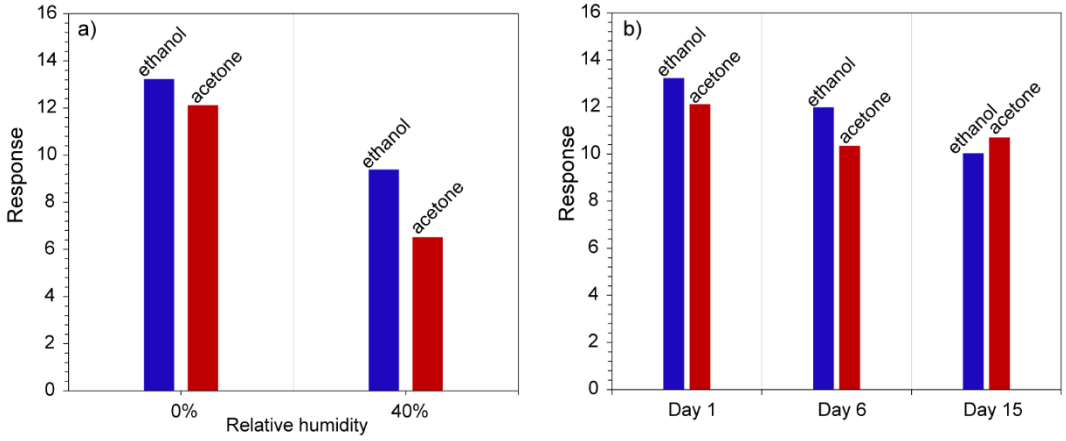

Figure S8: a) Effect of humidity on the response of NGP sensors toward 50ppm of ethanol and acetone at 200 °C. Clearly, NGP sensors response reduced under 40% of relative humidity, but still able to retain higher response as compared to bare NiO NWs in air at 200 °C. b) Stability of NGP toward 50ppm of ethanol and acetone (at 200 °C) over the period of 15 days. Evidently, NGP sensors exhibit stable performance with small fluctuation in response value.

1.11. Literature Comparison

The performance of GOPS-functionalized NiO NWs was also compared with the other ethanol and acetone sensors available in the literature (see table S2), focusing on the different strategies used to improve the sensing performance of NiO, like morphology (nanoparticles, nanorods, nanosheets, and nanofibers), heterostructure, doping, etc. Clearly, GOPS-functionalized NiO NWs showed superior performances in all aspects (detection of lower concentration, lower working temperature, and higher response) as compared to all the reports presented in table S2. For example, Al-doped NiO nanorods-flower showed comparable response values at the same temperature, but to a higher concentration of ethanol. On the other hand, in the reports[13,14] that showed higher response values than GOPS-functionalized sensors, the sensors were also operated at a higher temperature. Hence, this comparison suggests that surface functionalization of p-type metal oxides with SAM is a superior strategy to enhance the sensor response maintaining a lower working temperature.

Table S3. Comparison of SAMs functionalized (NGP) and NiO nanowires sensor performance with literature.

Material	**Strategies**	**Gas/Concentration (ppm)**	**Working temperature (˚C)**	**Response**	**Ref.**
NiO/ZnO	Branch-like heterostructure	Ethanol (50) Acetone (100	400	2.9 3.6	[15]
Al-doped NiO	Nanorods-flower	Ethanol (100)	200	12	[16]
Au-Functionalized NiO	Nanoparticles	Ethanol (1000)	325	4.4	[17]
Ultrathin and Porous NiO	Nanosheets	Acetone (0.2)	225	1.07	[18]
In_2O_3–NiO	Nanofibers	Acetone (50)	260	11.8	[19]
NiO	Flake-flower	Ethanol (400)	300	32	[14]
NiO–RuO_2	Nanoparticles	Ethanol (1000)	350	29.1	[13]
NiO	Nanowires	Ethanol (20, 50, 75)	200	1.6; 2.1; 2.3	This work
			500	5.6; 9.4; 11.2	
NiO	Nanowires	Acetone (20, 50, 75)	200	1.1; 1.8; 2.1	This work
			500	7.9;11.6;13.7	
NGP (GOPS-	Nanowires	Ethanol (20, 50, 75)	200	7.2; 13.2; 15.1	This

functionalized NiO)	Acetone (20, 50, 75)	200	5.3; 12.1; 17.8	work

References

1 M. Singh, N. Kaur, G. Drera, A. Casotto, L. S. Ermenegildo and E. Comini, *Adv. Funct. Mater.*, 2020, **30**, 2003217.

2 N. Kaur, E. Comini, D. Zappa, N. Poli and G. Sberveglieri, *Nanotechnology*, 2016, **27**, 205701.

3 N. Kaur, M. Singh and E. Comini, *Langmuir*, 2020, **36**, 6326–6344.

4 N. Kaur, E. Comini, D. Zappa, N. Poli and G. Sberveglieri, *Nanotechnology*, 2016, **27**, 205701.

5 M. Singh, N. Kaur and E. Comini, *J. Mater. Chem. C*, 2020, **8**, 3938–3955.

6 N. Kaur, D. Zappa and E. Comini, *Electron. Mater. Lett.*, 2019, **15**, 743–749.

7 N. Mironova-Ulmane, A. Kuzmin, I. Steins, J. Grabis, I. Sildos and M. Pärs, *J. Phys. Conf. Ser.*, 2007, **93**, 012039.

8 G. Drera, G. Salvinelli, J. Åhlund, P. G. Karlsson, B. Wannberg, E. Magnano, S. Nappini and L. Sangaletti, *J. Electron Spectros. Relat. Phenomena*, 2014, **195**, 109–116.

9 M. A. van Veenendaal and G. A. Sawatzky, *Phys. Rev. Lett.*, 1993, **70**, 2459–2462.

10 F. Parmigiani and L. Sangaletti, *J. Electron Spectros. Relat. Phenomena*, 1999, **98**–**99**, 287–302.

11 N. Pauly, F. Yubero, F. J. García-García and S. Tougaard, *Surf. Sci.*, 2016, **644**, 46–52.

12 I. Preda, R. J. O. Mossanek, M. Abbate, L. Alvarez, J. Méndez, A. Gutiérrez and L. Soriano, *Surf. Sci.*, 2012, **606**, 1426–1430.

13 V. Kruefu, A. Wisitsoraat, D. Phokharatkul, A. Tuantranont and S. Phanichphant, *Sensors Actuators B Chem.*, 2016, **236**, 466–473.

14 R. Miao and W. Zeng, *Mater. Lett.*, 2016, **171**, 200–203.

15 N. Kaur, D. Zappa, M. Ferroni, N. Poli, M. Campanini, R. Negrea and E. Comini, *Sensors Actuators B Chem.*, 2018, **262**, 477–485.

16 C. Wang, X. Cui, J. Liu, X. Zhou, X. Cheng, P. Sun, X. Hu, X. Li, J. Zheng and G. Lu, *ACS Sensors*, 2016, **1**, 131–136.

17 S. Park, H. Kheel, G.-J. Sun, S. K. Hyun, S. E. Park and C. Lee, *Bull. Korean Chem. Soc.*, 2016, **37**, 713–719.

18 C. Li, P. G. Choi, K. Kim and Y. Masuda, *Sensors Actuators B Chem.*, 2022, **367**, 132143.

19 X. Fan, Y. Xu and W. He, *RSC Adv.*, 2021, **11**, 11215–11223.